Nanoscale Research Letters
a SpringerOpen Journal

NANO REVIEW   **Open Access**

Effects of interdot hopping and Coulomb blockade on the thermoelectric properties of serially coupled quantum dots

David M T Kuo[1] and Yia-Chung Chang[2*]

Abstract

We have theoretically studied the thermoelectric properties of serially coupled quantum dots (SCQDs) embedded in an insulator connected to metallic electrodes. In the framework of Keldysh Green's function technique, the Landauer formula of transmission factor is obtained using the equation of motion method. Based on such analytical expressions of charge and heat currents, we calculate the electrical conductance, Seebeck coefficient, electron thermal conductance, and figure of merit (ZT) of SCQDs in the linear response regime. The effects of interdot hopping and electron Coulomb interactions on ZT are analyzed. We demonstrate that ZT is not a monotonic increasing function of interdot electron hopping strength (t_c). We also show that in the absence of phonon thermal conductance, SCQD can reach the Carnot efficiency as t_c approaches zero.

Review

Introduction

Recently, many considerable studies have been devoted to seeking efficient thermoelectric materials with the figure of merit (ZT) larger than 3 because there exist potential applications of solid-state thermal devices such as coolers and power generators [1-6]. Some theoretical efforts have pointed out that a single quantum dot (QD) junction system can have a very impressive ZT in the absence of phonon conductance [7-9]. However, in practice, it is difficult to maintain a large temperature gradient which is needed to produce sufficient temperature difference across the nanoscale junction. To reduce the temperature gradient across the QD junction, it is essential to consider many serially coupled quantum dots (SCQDs) [1,5]. The transport property of a junction involving N serially coupled QDs with strong electron Coulomb interactions is one of the most challenging topics of condensed matter physics. To gain some insight, we investigate in the present paper the thermoelectric effect of serially coupled quantum dots (SCQDs) as shown in the inset of Figure 1a.

It has been shown that the transport properties of the SCQD system exhibit several interesting features, including current rectification (due to the Pauli spin blockade), negative differential conductance, nonthermal broadening of tunneling current, and coherent tunneling in the Coulomb blockade regime [10]. Although many theoretical investigations of the above phenomena have been reported, most of them did not investigate the thermoelectric properties of SCQDs [11-13]. This study investigates the ZT of a SCQD embedded in a semiconductor nanowire with small phonon thermal conductance [4]. It is expected that the SCQD system has a potential to enhance the ZT of nanowires. Here, we consider nanoscale semiconductor QDs, in which the energy level separations are much larger than their on-site Coulomb interactions and thermal energies. Thus, only one energy level for each quantum dot needs to be considered. A two-level Anderson model [13] is employed to simulate the SCQD junction system.
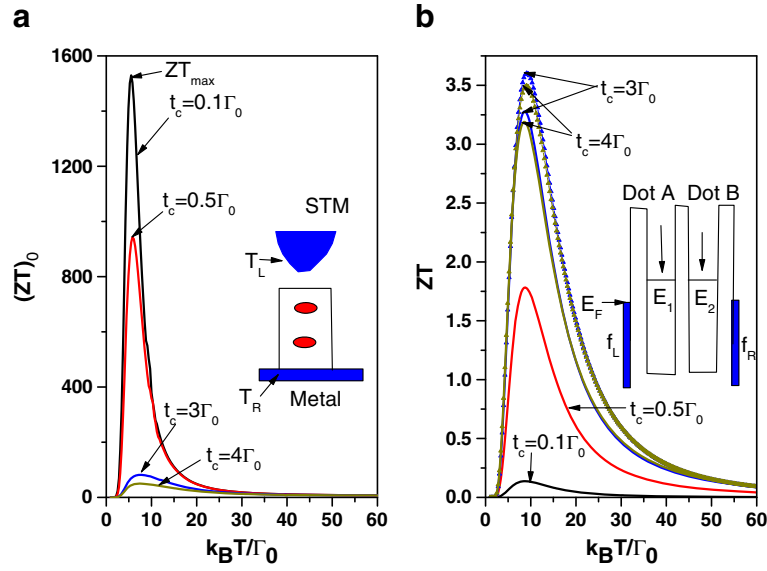
Theoretical model

Using Keldysh-Green's function technique [13], the charge and heat currents of SCQD connected to metallic electrodes are given by

$$J = \frac{2e}{h} \int d\epsilon \, \mathcal{T}(\epsilon) \left[f_L(\epsilon) - f_R(\epsilon) \right], \tag{1}$$

*Correspondence: yiachang@gate.sinica.edu.tw
[2]Research Center for Applied Sciences, Academic Sinica, Taipei, 115, Taiwan
Full list of author information is available at the end of the article

Figure 1 Functions of temperature. (**a**) $(ZT)_0$ and (**b**) ZT as functions of temperature for various interdot hopping strengths ($t_c = 0.1, 0.5, 1, 3,$ and $4\Gamma_0$). $E_\ell = E_F + 30\Gamma_0$, $U_\ell = 30\Gamma_0$, $U_{\ell,j} = 10\Gamma_0$, and $\Gamma_L = \Gamma = \Gamma_0$. STM, scanning tunneling microscope.

$$Q = \frac{2}{h} \int d\epsilon\, \mathcal{T}(\epsilon)(\epsilon - E_F - e\Delta V)\left[f_L(\epsilon) - f_R(\epsilon)\right], \quad (2)$$

where $\mathcal{T}(\epsilon) \equiv (\mathcal{T}_{12}(\epsilon) + \mathcal{T}_{21}(\epsilon))/2$ is the transmission factor. $f_{L=1(R=2)}(\epsilon) = 1/\left[e^{(\epsilon - \mu_{L(R)})/k_B T_{L(R)}} + 1\right]$ denotes the Fermi distribution function for the left (right) electrode. The left (right) chemical potential is given by $\mu_L(\mu_R)$. $T_{L(R)}$ denotes the equilibrium temperature of the left (right) electrode. e and h denote the electron charge and Planck's constant, respectively. $\mathcal{T}_{\ell,j}(\epsilon)$ denotes the transmission function, which can be calculated by evaluating the on-site retarded Green's function (GF) and lesser GF [13]. The indices ℓ and j denote the ℓth QD and the jth QD, respectively. Based on the equation of motion method, we can obtain analytical expressions of all GFs in the Coulomb blockade regime. Details are provided in [13]. The transmission function in the weak interdot limit ($t_c/U_\ell \ll 1$, where t_c and U_ℓ denote the electron interdot hopping strength and on-site Coulomb interaction, respectively) can be recast into the following form:

$$\mathcal{T}_{\ell,j}(\epsilon) = -2\sum_{m=1}^{8} \frac{\Gamma_\ell(\epsilon)\Gamma_j^m(\epsilon)}{\Gamma_\ell(\epsilon) + \Gamma_j^m(\epsilon)} \mathrm{Im}G_{\ell,m,\sigma}^r(\epsilon), \quad (3)$$

where Im means taking the imaginary part of the function that follows and

$$G_{\ell,m,\sigma}^r(\epsilon) = p_m/(\mu_\ell - \Sigma_m). \quad (4)$$

$\Gamma_{\ell=L(1),R(2)}(\epsilon)$ denotes the tunnel rate from the left electrode to dot A (E_1) and the right electrode to dot B (E_2), which is assumed to be energy- and bias-independent for simplicity. $\mu_\ell = \epsilon - E_\ell + i\Gamma_\ell/2$. We can assign the following physical meaning to Equation 3. The sum in

Equation 3 is over eight possible configurations labeled by m. We consider an electron (of spin σ) entering level ℓ, which can be either occupied (with probability $N_{\ell,\bar\sigma}$) or empty (with probability $1 - N_{\ell,\bar\sigma}$). For each case, the electron can hop to level j, which can be empty (with probability $a_j = 1 - N_{j,\sigma} - N_{j,\bar\sigma} + c_j$), singly occupied in a spin $\bar\sigma$ state (with probability $b_{j,\bar\sigma} = N_{j,\bar\sigma} - c_j$) or spin σ state (with probability $b_{j,\sigma} = N_{j,\sigma} - c_j$), or a double-occupied state (with probability c_j). Thus, the probability factors associated with the eight configurations appearing in Equation 4 become $p_1 = (1 - N_{\ell,\bar\sigma})a_j$, $p_2 = (1 - N_{\ell,\bar\sigma})b_{j,\bar\sigma}$, $p_3 = (1 - N_{\ell,\bar\sigma})b_{j,\sigma}$, $p_4 = (1 - N_{\ell,\bar\sigma})c_j$, $p_5 = N_{\ell,\bar\sigma}a_j$, $p_6 = N_{\ell,\bar\sigma}b_{j,\bar\sigma}$, $p_7 = N_{\ell,\bar\sigma}b_{j,\sigma}$, and $p_8 = N_{\ell,\bar\sigma}c_j$. Σ_m in the denominator of Equation 4 denotes the self-energy correction due to Coulomb interactions and coupling with level j (which couples with the other electrode) in configuration m. We have $\Sigma_1 = t_c^2/\mu_j$, $\Sigma_2 = U_{\ell,j} + t_c^2/(\mu_j - U_j)$, $\Sigma_3 = U_{\ell,j} + t_c^2/(\mu_j - U_{j,\ell})$, $\Sigma_4 = 2U_{\ell,j} + t_c^2/(\mu_j - U_j - U_{j,\ell})$, $\Sigma_5 = U_\ell + t_c^2/(\mu_j - U_{j,\ell})$, $\Sigma_6 = U_\ell + U_{\ell,j} + t_c^2/(\mu_j - U_j - U_{j,\ell})$, $\Sigma_7 = U_\ell + U_{\ell,j} + t_c^2/(\mu_j - 2U_{j,\ell})$, and $\Sigma_8 = U_\ell + 2U_{\ell,j} + t_c^2/(\mu_j - U_j - 2U_{j,\ell})$. E_ℓ, U_ℓ, and $U_{\ell,j}$ denote, respectively, the energy levels of dots, intradot Coulomb interactions, and interdot Coulomb interactions. Here, $\Gamma_j^m = -2\mathrm{Im}\Sigma_j$ denotes the effective tunneling rate from level l to the other electrode through level j in configuration m. For example, $\Gamma_j^1 = -2\mathrm{Im}\, t_c^2/\mu_j = t_c^2\Gamma_j/\left[(\epsilon - E_j)^2 + (\Gamma_j/2)^2\right]$. It is noted that Γ_j^m has a numerator Γ_j for all configurations. Furthermore, $G_{\ell,\sigma}^r(\epsilon) = \sum_{m=1}^{8} G_{\ell,m,\sigma}^r(\epsilon)$ is just the on-site single-particle retarded GF for level ℓ as given in Equation (A16) of [13], and $G_{\ell,m,\sigma}^r(\epsilon)$ corresponds to its partial GF in configuration m. The transmission function written this

way has the same form as Landauer's formula for a single QD with multiple energy levels including intralevel and interlevel electron Coulomb interactions [14,15].

The probability factors of Equation 3 are determined by the thermally averaged one-particle occupation number and two-particle correlation functions, which can be obtained by solving the on-site lesser Green's functions [13]:

$$N_{\ell,\sigma} = -\int \frac{d\epsilon}{\pi} \sum_{m=1}^{8} \frac{\Gamma_\ell f_\ell(\epsilon) + \Gamma_j^m f_j(\epsilon)}{\Gamma_\ell + \Gamma_j^m} \text{Im} G_{\ell,m,\sigma}^r(\epsilon),$$

(5)

and

$$c_\ell = -\int \frac{d\epsilon}{\pi} \sum_{m=5}^{8} \frac{\Gamma_\ell f_\ell(\epsilon) + \Gamma_j^m f_j(\epsilon)}{\Gamma_\ell + \Gamma_j^m} \text{Im} G_{\ell,m,\sigma}^r(\epsilon). \quad (6)$$

Note that $\ell \neq j$ in Equations 3, 5, and 6. In the linear response regime, Equations 1 and 2 can be rewritten as follows:

$$J = \mathcal{L}_{11} \frac{\Delta V}{T} + \mathcal{L}_{12} \frac{\Delta T}{T^2}$$

(7)

$$Q = \mathcal{L}_{21} \frac{\Delta V}{T} + \mathcal{L}_{22} \frac{\Delta T}{T^2},$$

(8)

where $\Delta V = \mu_L - \mu_R$ and $\Delta T = T_L - T_R$ are the voltage and temperature differences across the junction, respectively. Thermoelectric response functions in Equations 7 and 8 are given by

$$\mathcal{L}_{11} = \frac{2e^2 T}{h} \int d\epsilon \mathcal{T}(\epsilon) \left(\frac{\partial f(\epsilon)}{\partial E_F} \right)_T,$$

(9)

$$\mathcal{L}_{12} = \frac{2e T^2}{h} \int d\epsilon \mathcal{T}(\epsilon) \left(\frac{\partial f(\epsilon)}{\partial T} \right)_{E_F},$$

(10)

$$\mathcal{L}_{21} = \frac{2e T}{h} \int d\epsilon \mathcal{T}(\epsilon)(\epsilon - E_F) \left(\frac{\partial f(\epsilon)}{\partial E_F} \right)_T,$$

(11)

and

$$\mathcal{L}_{22} = \frac{2 T^2}{h} \int d\epsilon \mathcal{T}(\epsilon)(\epsilon - E_F) \left(\frac{\partial f(\epsilon)}{\partial T} \right)_{E_F}. \quad (12)$$

Here, $\mathcal{T}(\epsilon)$ and $f(\epsilon) = 1/\left[e^{(\epsilon - E_F)/k_B T} + 1\right]$ are evaluated in the equilibrium condition. It can be shown that the Onsager relation $\mathcal{L}_{12} = \mathcal{L}_{21}$ is preserved. These thermoelectric response functions can also be found in [7], where authors investigated the thermoelectric properties of a single QD.

If the system is in an open circuit, the electrochemical potential will form in response to a temperature gradient; this electrochemical potential is known as the Seebeck voltage (Seebeck effect). The Seebeck coefficient (amount of voltage generated per unit temperature gradient) is defined as $S = \Delta V/\Delta T = -\mathcal{L}_{12}/(T\mathcal{L}_{11})$. To judge whether the system is able to generate power or refrigerate efficiently, we need to consider the figure of merit, which is given by

$$ZT = \frac{S^2 G_e T}{\kappa_e + \kappa_{ph}} \equiv \frac{(ZT)_0}{1 + \kappa_{ph}/\kappa_e}. \quad (13)$$

Here, $G_e = \mathcal{L}_{11}/T$ is the electrical conductance, and $\kappa_e = ((\mathcal{L}_{22}/T^2) - \mathcal{L}_{11}S^2)$ is the electron thermal conductance. $(ZT)_0$ represents the ZT value in the absence of phonon thermal conductance, κ_{ph}. For simplicity, we assume $\kappa_{ph} = \kappa_{ph,0} F_s$ [16-18]. $\kappa_{ph,0} = \frac{\pi^2 k_B^2 T}{3h}$ is the universal phonon thermal conductance arising from acoustic phonon confinement in a nanowire [16-18], which was confirmed in the phonon wave guide [19]. The expression of $\kappa_{ph} = \kappa_{ph,0} F_s$ with $F_s = 0.1$ can explain well the phonon thermal conductance of silicon nanowire with surface states calculated by the first-principles method [16]. The dimensionless scattering factor F_s arises from phonon scattering with surface impurities or surface defects of quantum dots [1,16]. Here, we adopt $F_s = 0.02$, which is smaller than $F_s = 0.1$ because QDs can enhance the phonon scattering rates and reduce phonon thermal conduction as pointed out in [1].

Results and discussion

Here, we consider the case of identical QDs in the optimization of ZT, although it is understood that the size fluctuation of QDs can suppress ZT [13]. In Figure 1a,b we plot $(ZT)_0$ and ZT as a function of temperature for various electron hopping strengths. We adopt the following physical parameters: $E_\ell = E_F + 30\Gamma_0$, $U_\ell = 30\Gamma_0$, $U_{\ell,j} = 10\Gamma_0$, and $\Gamma_L = \Gamma_R = \Gamma = 1\Gamma_0$. All energy scales are in the units of the characteristic energy, Γ_0. In Figure 1a, we see that $(ZT)_0$ increases with decreasing t_c and diverges as $t_c \to 0$. This behavior can be proved rigorously as we shall illustrate below. It implies that SCQD can reach the Carnot efficiency in the limit of extremely weak interdot coupling, if one can fully suppress κ_{ph}, for example, by inserting a nanoscale vacuum layer to block the phonon heat current. Although it would be a challenging task to implement a vacuum layer between one of the electrodes and SCQD, it may be possible to test this idea out via a scanning tunneling microscopic experiment using a setup as shown in the inset of Figure 1a. In Figure 1b, we see that ZT is enhanced with increasing t_c until t_c reaches $3\Gamma_0$, and it becomes reduced for higher t_c.

The diverging behavior of $(ZT)_0$ with respect to t_c is further illustrated in Figure 2d. The maximum ZT is suppressed in the presence of κ_{ph}, which is much larger than κ_e for small t_c. The behaviors of ZT shown in Figure 1b are mostly determined by the power factor ($S^2 G_e$). Once t_c is larger than $3\Gamma_0$, the reduction of S^2 is faster than the increase of G_e. This explains why the maximum ZT at
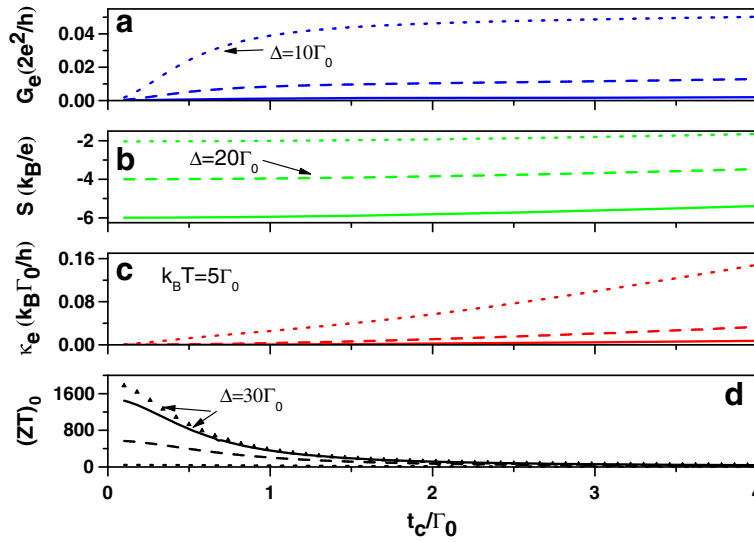
Figure 2 Functions of t_c at $k_B T = 5\Gamma_0$. (**a**) Electrical conductance (G_e), (**b**) Seebeck coefficient (S), (**c**) electrical thermal conductance (κ_e), and (**d**) $(ZT)_0$ as functions of t_c at $k_B T = 5\Gamma_0$ for $\Delta = 10\Gamma_0$ (dotted curves), $20\Gamma_0$ (dashed curves), and $30\Gamma_0$ (solid curves). Other parameters are the same as those of Figure 1.

$t_c = 4\Gamma_0$ is smaller than that at $t_c = 3\Gamma_0$. The location of ZT_{max} is nearly independent of t_c, and it occurs near $k_B T = 8.8\Gamma_0$. For comparison, we also show the results (curves with triangle marks) for the case without electron Coulomb interactions in Figure 1b. It is seen that the maximum ZT is enhanced when we turn off the electron Coulomb interactions. Such a behavior is similar to that of a single QD with multiple energy levels [7,8]. The effect of electron Coulomb interactions is significant only for temperature between $6\Gamma_0$ and $50\Gamma_0$. Namely, the electron Coulomb interactions are negligible when $U/(k_B T) \gg 1$ or $U/(k_B T) \ll 1$.

To further understand the behavior of ZT with respect to t_c, we plot the electrical conductance (G_e), Seebeck coefficient (S), electrical conductance κ_e, and $(ZT)_0$ as functions of t_c in Figure 2 for various detuning energies, $\Delta \equiv E_\ell - E_F$. When E_ℓ is close to the Fermi energy, G_e and κ_e are enhanced, whereas S and $(ZT)_0$ are suppressed. The behavior of $(ZT)_0$ at $\Delta = 30\Gamma_0$ in the absence of Coulomb interactions is also shown by the curve with triangles, which has a similar trend as the solid line. Thus, it is instructive to analyze $(ZT)_0$ in the absence of Coulomb interactions. Keeping the leading order of t_c^2, we have $\mathcal{L}_{11} = \frac{2e^2}{h k_B} \frac{t_c^2}{\Gamma_0/2} \frac{1}{\cosh^2(\Delta/2 k_B T)}$, $\mathcal{L}_{12} = \mathcal{L}_{21} = \frac{2e}{h k_B} \frac{t_c^2}{\Gamma_0/2} \frac{\Delta}{\cosh^2(\Delta/2 k_B T)}$, and $\mathcal{L}_{22} = \frac{2}{h k_B} \frac{t_c^2}{\Gamma_0/2} \frac{\Delta^2}{\cosh^2(\Delta/2 k_B T)}$. Therefore, $G_e \propto t_c^2$, $S = -\Delta/eT$ is independent on t_c, and $\kappa_e = (\mathcal{L}_{22} - \mathcal{L}_{12}^2/\mathcal{L}_{11})/T^2$ vanishes up to t_c^2. Thus, the leading order of κ_e is t_c^4. This indicates that $(ZT)_0 \propto 1/t_c^2$ in the limit of weak interdot hopping.

Figure 3 shows ZT as a function of $\Delta = E_\ell - E_F$ for various electron hoping strengths at $k_B T = 10\Gamma_0$.

Other physical parameters are kept the same as those for Figure 1. When $t_c = 0.1\Gamma_0$, the maximum ZT (ZT_{max}) occurs at near $\Delta = 27\Gamma_0$. The peak position only shifts slightly to higher Δ with increasing t_c. We have $ZT_{max} = 2.79$ and 3.18 for $t_c = 1\Gamma_0$ and $3\Gamma_0$, respectively. However, at $t_c = 4\Gamma_0$, we have $ZT_{max} = 3.07$, which is smaller than ZT_{max} for $t_c = 3\Gamma_0$. Thus, it also illustrates that ZT is not a monotonically increasing function of t_c. We further calculated ZT as a function of t_c for $\Delta = 10, 20, 30\Gamma_0$ and $k_B T = 10\Gamma_0$ in the presence of κ_{ph} and found that again, ZT is not a monotonically increasing function of t_c (not shown here). We conclude that as long as κ_{ph} dominates over κ_e, the t_c dependence of ZT is mainly determined by the power factor $S^2 G_e$, where the behaviors of G_e and S are similar to the results shown in Figure 2a,b. When $t_c/\Gamma_0 \leq 1$, G_e increases much faster than the reduction of S^2 for increasing t_c, and the power factor slowly reaches the maximum when t_c approaches $3\Gamma_0$. When $t_c > 3\Gamma_0$, the power factor decreases due to the fast reduction of S^2 which prevails over the increase of G_e. The curve with triangle marks is for $t_c = 3\Gamma_0$ in the absence of Coulomb interaction. We see that ZT_{max} is larger when $U_\ell = U_{\ell,j} = 0$. Based on the results of Figure 3, we conclude that it is important to control the detuning energy Δ for the optimization of ZT.

In Figures 1, 2, and 3 we have considered the case with E_F below QD energy levels. It would be interesting to investigate the case with E_F above the energy levels of QDs. Figure 4 shows G_e, S, κ_e, and ZT of an SCQD with $t_c = 3\Gamma_0$ as functions of applied gate voltage for various temperatures. Once $t_c > (\Gamma_L + \Gamma_R) = 2\Gamma_0$, the eight peaks for G_e can be resolved at $k_B T = 1\Gamma_0$. These eight peaks
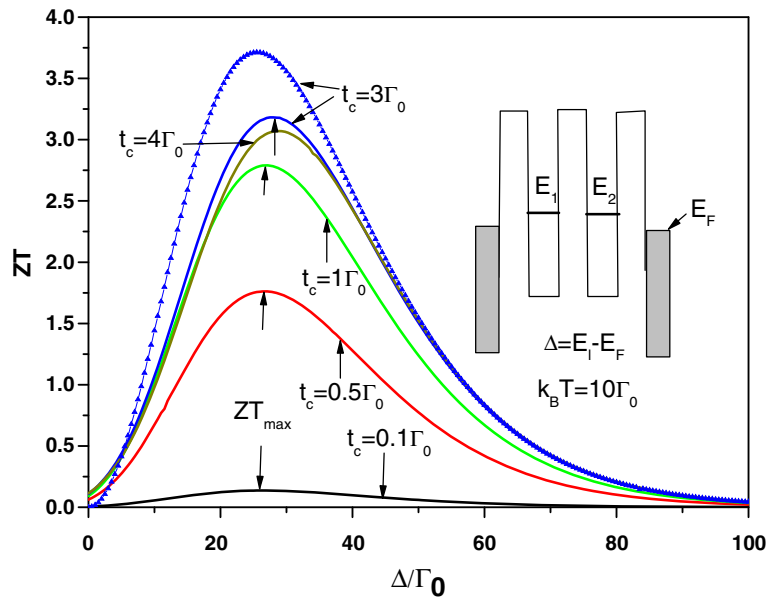
Figure 3 ZT as a function of Δ for different electron hopping strength at $k_B T = 10\Gamma_0$. Other parameters are the same as those of Figure 1.
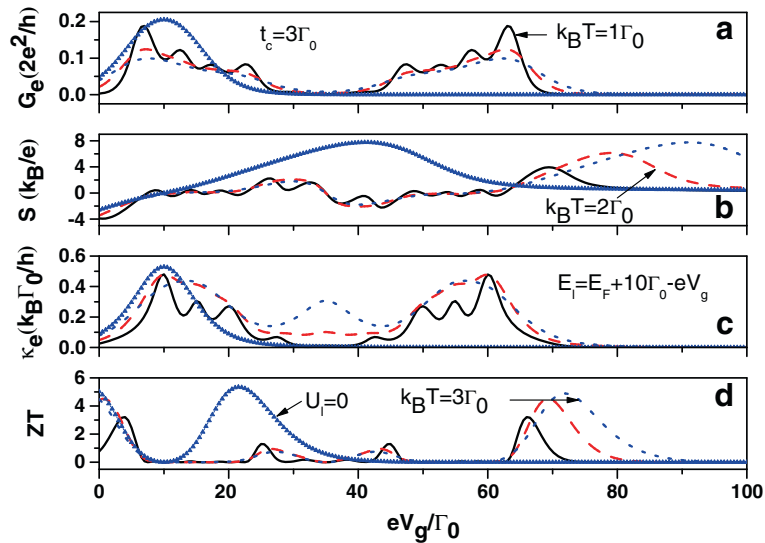
Figure 4 Function of applied gate voltage. (**a**) G_e, (**b**) S, (**c**) κ_e, and (**d**) ZT as a function of applied gate voltage for $k_B T = 1\Gamma_0$ (solid), $2\Gamma_0$ (dashed), and $3\Gamma_0$ (dotted). $E_\ell = E_F + 10\Gamma_0$ and $t_c = 3\Gamma_0$. Other parameters are the same as those of Figure 1. The curves with triangle marks are for the case without electron Coulomb interactions for $k_B T = 3\Gamma_0$.

correspond to the following resonant channels: $E_\ell - t_c$, $E_\ell + t_c$, $E_\ell + U_{\ell,j} - t_c$, $E_\ell + U_{\ell,j} + t_c$, $E_\ell + U_{\ell,j} + U_\ell - t_c$, $E_\ell + U_{\ell,j} + U_\ell + t_c$, $E_\ell + 2U_{\ell,j} + U_\ell - t_c$, and $E_\ell + 2U_{\ell,j} + U_\ell + t_c$, which are tuned by the gate voltage to be aligned with E_F. These eight channels result from the four configurations of p_1, p_3, p_6, and p_8 in Equation 4. Such a result implies that SCQD with identical QDs acts as a QD with effective two levels of $E_\ell - t_c$ and $E_\ell + t_c$ and satisfying Hund's rule.

These eight peaks are smeared out with increasing temperature. The sign changes of S with respect to the gate voltage result from the bipolar effect, i.e., the competition between electrons and holes, where holes are defined as the unoccupied states below E_F [13]. The electronic thermal conductance (κ_e) also exhibits eight peaks, and we noticed that the local maxima of the κ_e curve nearly coincide with the local minima of the G_e curve. We see that ZT

values are still larger than 3 even when E_ℓ is deeply below E_F (say, at $eV_g = 70\Gamma_0$). This is attributed to the electron Coulomb interaction. To illustrate that, we also show the results with $U_\ell = U_{\ell,j} = 0$ at $k_B T = 3\Gamma_0$ (see the curve with triangle marks). The oscillation of ZT in the case of $U_\ell = U_{\ell,j} = 0$ is attributed to the sign change of S at $V_g = 10\Gamma_0$. Note that S goes to zero at $V_g = 10\Gamma_0$, which results from the electron-hole symmetry (with $E_\ell + t_c$ and $E_\ell - t_c$ straddling E_F symmetrically). We see that ZT vanishes for $eV_g \geq 40\Gamma_0$ in the absence of electron Coulomb interactions. Unlike the case of $E_F < E_\ell$, where the finite U causes reduction of ZT, here, the electron Coulomb interaction leads to enhancement of ZT when $E_F > E_\ell$.

Conclusions

In summary, the thermoelectric properties including G_e, S, κ_e, and ZT of the SCQD junction system are investigated theoretically. We demonstrate that the Carnot efficiency can be reached when t_c approaches zero in the absence of phonon thermal conductance. When the phonon contribution dominates the thermal conductance of the SCQD junction, the optimization of ZT can be obtained by the thermal power defined as $S^2 G_e$. We also found that the presence of electron Coulomb interactions can lead to either reduction or enhancement of ZT, depending on whether the Fermi level is below or above the QD level.

Competing interests
The authors declare that they have no competing interests.

Authors' contributions
DMTK and Y-CC established the theoretical formalism. DMTK carried out the numerical calculations and drafted the manuscript. Y-CC conceived this study and participated in its coordination. All authors read and approved the final manuscript.

Authors' information
DMTK received his Ph.D. degree from National Taiwan University in 1996. He joined the Department of Electrical Engineering, National Central University in 2003 as an assistant professor, became an associate professor in 2005, and professor in 2008. His main research interests include nanodevices and quantum transport.
Y-CC received his Ph.D. degree from the California Institute of Technology in 1980. He joined the Physics Department, University of Illinois at Urbana-Champaign in 1980 as a visiting research assistant professor and became an assistant professor in 1982, associate professor in 1986, and professor in 1991. In 2005, he joined Academia Sinica, Taiwan as a Distinguished Research Fellow of the Research Center for Applied Sciences. His main research interests include condensed matter theory, semiconductor electronics, photonic materials, and optoelectronic devices.

Author details
^{1}Department of Electrical Engineering and Department of Physics, National Central University, Chungli, 320, Taiwan. ^{2}Research Center for Applied Sciences, Academic Sinica, Taipei, 115, Taiwan.

References
1. Minnich AJ, Dresselhaus MS, Ren ZF, Chen G: **Bulk nanostructured thermoelectric materials: current research and future prospects.** *Energy Environ Sci* 2009, **2**:466–479.
2. Mahan G, Sales B, Sharp J: **Thermoelectric materials: new approaches to an old problem.** *Physics Today* 1997, **50**(3):42–47.
3. Venkatasubramanian R, Siivola E, Colpitts T, O'Quinn B: **Thin-film thermoelectric devices with high room-temperature figures of merit.** *Nature* 2001, **413**:597–602.
4. Boukai AI, Bunimovich Y, Tahir-Kheli J, Yu JK, Goddard IIIWA, Heath JR: **Silicon nanowires as efficient thermoelectric materials.** *Nature* 2008, **451**:168–171.
5. Harman TC, Taylor PJ, Walsh MP, LaForge BE: **Quantum dot superlattice thermoelectric materials and devices.** *Science* 2002, **297**:2229–2232.
6. Hsu KF, Loo S, Guo F, Chen W, Dyck JS, Uher C, Hogan T, Polychroniadis EK, Kanatzidis MG: **Cubic AgPbmSbTe2+m: bulk thermoelectric materials with high figure of merit.** *Science* 2004, **303**:818–821.
7. Murphy P, Mukerjee S, Moore J: **Optimal thermoelectric figure of merit of a molecular junction.** *Phys Rev B* 2008, **78**:161406–161410.
8. Kuo DMT, Chang YC: **Thermoelectric and thermal rectification properties of quantum dot junctions.** *Phys Rev B* 2010, **81**:205321–205331.
9. Dubi Y, Di Ventra M: **Heat flow and thermoelectricity in atomic and molecular junctions.** *Rev Modern Phys* 2011, **83**:131–155.
10. Ono K, Austing DG, Tokura Y, Tarucha S: **Current rectification by Pauli exclusion in a weakly coupled double quantum dot system.** *Science* 2002, **297**:1313–1317.
11. Fransson J, Rasander M: **Pauli spin blockade in weakly coupled double quantum dots.** *Phys Rev B* 2006, **73**:205333–205342.
12. Sun QF, Xing Y, Shen SQ: **Double quantum dot as detector of spin bias.** *Phys Rev B* 2008, **77**:195313.
13. Kuo DMT, Shiau SY, Chang YC: **Theory of spin blockade, charge ratchet effect, and thermoelectrical behavior in serially coupled quantum dot system.** *Phys Rev B* 2011, **84**:245303–245314.
14. Kuo DMT, Chang YC: **Tunneling current spectroscopy of a nanostructure junction involving multiple energy levels.** *Phys Rev Lett* 2007, **99**:086803–086807.
15. Chang YC, Kuo DMT: **Theory of charge transport in a quantum dot tunnel junction with multiple energy levels.** *Phys Rev B* 2008, **77**:245412–245428.
16. Markussen T, Jauho AP, Brandbyge M: **Surface-decorated silicon nanowires: a route to high-ZT thermoelectrics.** *Phys Rev Lett* 2009, **103**:055502–055506.
17. Santamore DH, Cross MC: **Effect of phonon scattering by surface roughness on the universal thermal conductance.** *Phys Rev Lett* 2001, **87**:115502–115506.
18. Rego LGC, Kirczenow G: **Quantized thermal conductance of dielectric quantum wires.** *Phys Rev Lett* 1998, **81**:232–236.
19. Schwab K, Henriksen EA, Worlock JM, Roukes ML: **Measurement of the quantum of thermal conductance.** *Nature* 2000, **404**:974–977.